Thesis

Arm Length Compensation System for Underground Gravitational-wave Telescope

Koseki Miyo

Department of Physics
University of Tokyo

MMM 2020

Contents

Chapter 1

Background

1.1 Gravitational-wave

1.1.1 ...

1.2 Sources of gravitational-wave

1.2.1 ...

1.3 Interferometric Gravitational-wave detection

1.3.1 ...

1.4 Terrestrial Laser Interferometers

1.4.1 ...

1.5 Under Ground Laser Interferometer

1.5.1 ...

1.6 Summary of the Chapter

Chapter 2

KAGRA

2.1 Overview

2.1.1 ...

2.1.2 ...

2.2 KAGRA Tunnel

2.2.1 Tunnel Design

KAGRA tunnel is excavated in the Kamioka mine in Hida, Gifu, Japan [1]. The tunnel is consisted of two floors. 干渉計を構成するほとんどの鏡は 1 階に設置された防振装置で懸架されているが、腕共振器を構成する 4 つの鏡は 1 階から 14m の高さにある 2 階から懸架されている。

The tunnel is locate under 200 m from ground surface to decrease the seismic noise effectively.

2.2.2 Geological features

Hida region to which Kamioka belongs is a ancient region in Japan island [2].

The main bedrock is the geniss.

2.3 Main Interferometer

2.3.1 Overview

KAGRA is a cryogenic intergerometric gravitational-wave detector constructed at the underground site of Kamioka mine [3].

2.3.2 Main Interferometer

Design

The design of KAGRA interferometer is dual recycled Fabry-Perot Michelson interferometer [4][5].

2.4 Vibration Isolation System

2.4.1 Overview

KAGRA has 4 types vibration isolation system.

2.4.2 Type-A Suspension System

Type-A suspensions are developed [6].

2.5 Summary of the Chapter

Chapter 3

Underground Seismic Noise

3.1 Seismic Noise

3.1.1 Overview

...
...
...
...
...
...

3.1.2 Microseisms

Microseisms which power spectrum has peaks in 50–200 mHz are excitated by oceanic waves. These seismic waves can be categolized by the generating mechanism of these [7].

The primary ocean microseisms are generated only in shallow waters in coastal regions. In this regions, the water wave enery can be converted directly into seismic energy either through vertical water pressure variations, or by the impacts of surf on the shores. There are correlation between this microseismic peak and the swell at the beaches was known starting from the data sets studied by [8].
...
...

The secondary ocean microseisms could be explained by the superposition of ocean waves of equal period traveling in opposite directions. Therefore, generating standing gravity waves of half the period [9].
...
...

The RMS amplitude spectral of both type of the microseisms are strongly depends on the low pressure on the ocean.
...
...

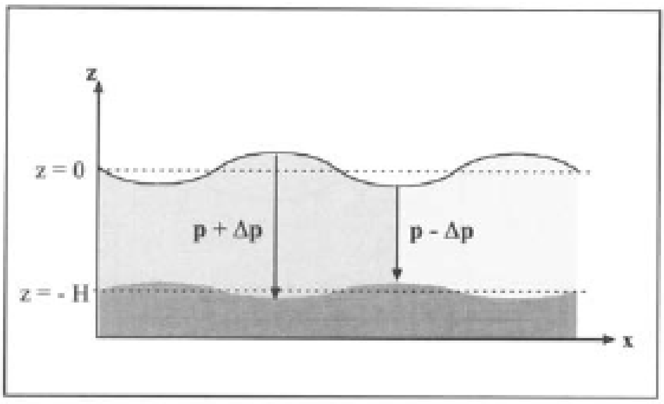

(a) Generating mechanism of the primary microseisms.

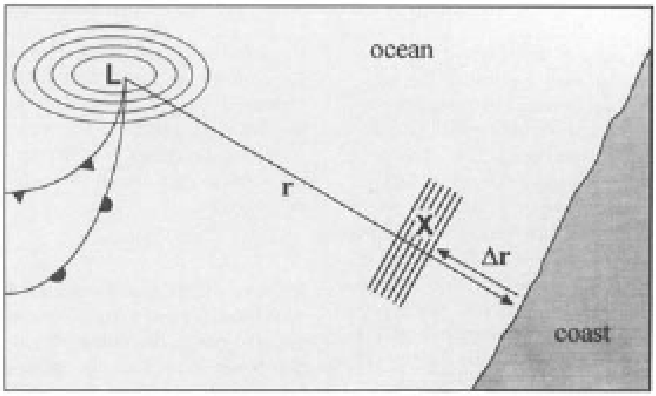

(b) Generating mechanism of the secondary microseisms.

Figure 3.1: Generating mechanism of the microsisms. (a) describes the mechanism of the primary microseisms. (b) describes the mechanism of the secondary microseisms.

3.1.3 Earthquakes

(Write how earthquakes disturb the large scale interferometer.)

Mechanism

遠方での大きな地震は脈動帯域以下の低周波地面振動を励起し、ロックロスの原因になる。

Early Earthquake Alert

Seismon をつかって到来時間を予測し、この低周波地面振動の RMS を抑えるための特別なフィルターに切り替えて、ロックロスをへらす工夫を行っている。しかし、このフィルターは脈動がうるさいときは再びロックロスの問題を抱えてしまう。

3.1.4 Earth Tides

3.2 Long-term Study of the seismic environment at KAGRA

3.2.1 Overview

3.2.2 Experimental Arrangement

Seismic motion ware acquired using seismometer which is installed on the second floor of the X-end named EXV are. The EXV area is placed under 200 m from surface of the mountain, and moreover, there are no entrance connected to the outside of the mountain in contrast both the Y-end and Corner area. Therefore, It is can be said that this area relatively quiet area in KAGRA site.

The seismometer is Trillium 120-QA whose three outputs are proportional to the ground velocity of two horizontal and one vertical respectively. As shown in fig. 3.2, the seismometer is covered by the black thermal insulator to reduce the thermal fluctuation. 温度のカップリングについてマニュアル chap3.3 を参考にして書く [10].

Figure 3.2: Trillium 120-QA installed on the second floor at X-end area named EXV area.

3.2.3 Data Aquisition

The spectra taken in almost 1 year period using a seismometer at 2nd floor in the X-end station.

3.2.4 Results

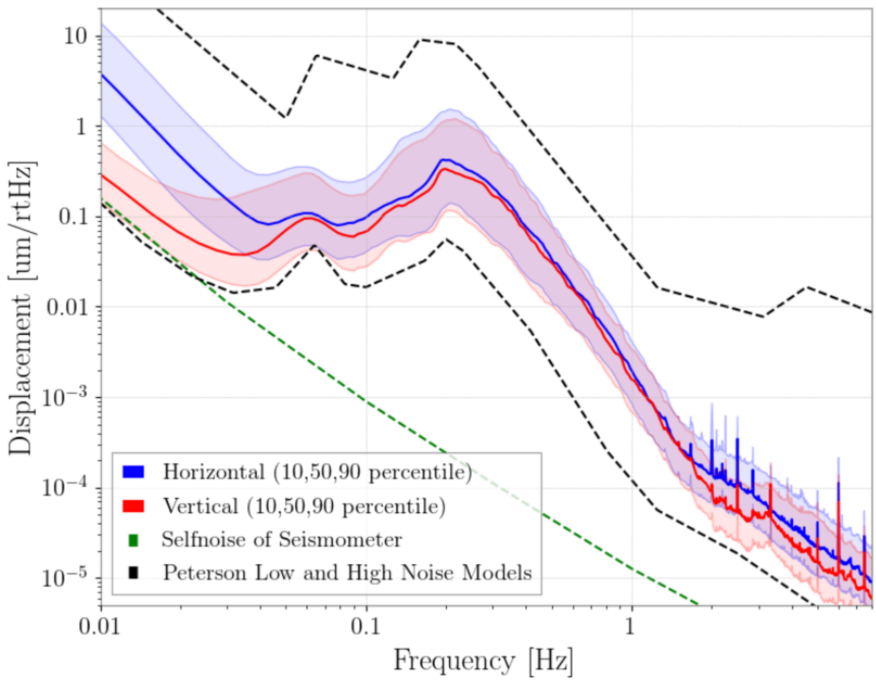

Figure 3.3

huge
...
...

3.2.5 Comparison to Other Site

3.3 Differential Motion Reduction

3.3.1 Introduction

The motion of two mirrors in the cavity have two modes. One is differential motion, which is the length change of that. Another one is common motion, which is the motion of the center of the cavity. In terms of the length control, it is important that the RMS amplitude of differential motion is as small as possible. Actuarlly, the amplitude of these two motions are the same each other when the mirrors moves with no coherence. However, when a coherence exists, the common motion tends to be larger than the differential one.

As discussed in this section, the coherence depends on both, the arm length and the wavelength of seismic waves. For example, if the arm length is much more smaller than the wavelength, the mirrors move together. This means that the common motion is greater than the differential motion.

The ratio of the amplitudes of the differential motion over common motion is newly defined as Common and Differential Motion Ratio (CDMR). It is usefull to know how the ground reducts the differential motion or increase the common motion.

3.3.2 Differential Motion Reduction

Differential Motion and Common Motion

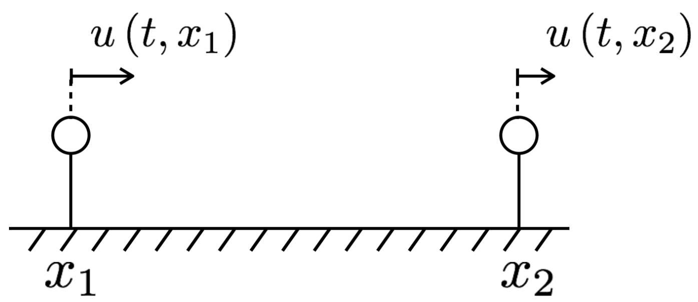

Figure 3.4: The displacements of the two points which are sparated L in X axis.

Motions of the two points can be represented as the differential motion and the common motion. Displacement of both differential motion and common motion of the two points shown in Figure(**??**) are defined as

$$u_{\text{diff}} \equiv \frac{u_1 - u_2}{\sqrt{2}},\ u_{\text{comm}} \equiv \frac{u_1 + u_2}{\sqrt{2}} \tag{3.1}$$

where $u_1(x,t)$ and $u_2(x,t)$ are the displacement of each points. These two motions defined in Eq.(3.1) are normalized by $\sqrt{2}$ due to conserve the total power.

Common and Differential Motion Ratio (CDMR)

CDMR is defined as the powers of common motion over the differential motion as bellow,

$$\text{CDMR} \equiv \sqrt{\frac{\text{Common Motion}}{\text{Differential Motion}}} = \sqrt{\frac{P_{\text{comm}}(\omega)}{P_{\text{diff}}(\omega)}} \tag{3.2}$$

where $P_{\text{comm}}, P_{\text{diff}}$ are the power spectral densities (PSDs) of the differential motion and common motion, respectively. Each PSDs are converted from the autocorrelation function of these by the Wiener-Khinchin theorem.

First, autocorrelation function C_{diff} of the differential motion is given by its definition in Eq.(3.1)

$$\begin{aligned} C_{\text{diff}}(\tau) &= \frac{1}{2}\left\langle \Big[x_1(t) - x_2(t)\Big]\Big[x_1(t+\tau) - x_2(t+\tau)\Big]\right\rangle & (3.3)\\ &= \frac{1}{2}\Big[C_{11}(\tau) - C_{12}(\tau) - C_{21}(\tau) + C_{22}(\tau)\Big], & (3.4)\end{aligned}$$

,where C_{ij} are the autocorrelation functions of each point and defined as $C_{ij} \equiv \langle x_i(t)x_j(t+\tau)\rangle$, $(i = 1,2,\ j = 1,2)$. Therefore, the power spectrum density of differential motion $P_{\text{diff}}(\omega)$ can be computed as

$$\begin{aligned} P_{\text{diff}}(\omega) &= \frac{1}{2}\Big[P_1(\omega) + P_2(\omega) - P_{12}(\omega) - P_{12}^*(\omega)\Big] & (3.5)\\ &= \frac{1}{2}\Big[P_1 + P_2 - \text{Re}\,[\gamma] \times 2\sqrt{P_1 P_2}\Big] & (3.6)\end{aligned}$$

where $P_1(\omega), P_2(\omega)$ are the power spectrum densities of each points, and $P_{12}(\omega)$ are the cross spectrum between two point. The parameter γ is the complex coherence between them defined below,

$$\gamma \equiv \frac{P_{12}}{\sqrt{P_1 P_2}}. \tag{3.7}$$

Here, assuming that seismic wave propagating each points does not decay, which means $P_1 = P_2 \equiv P$, one can compute the $P_{\text{diff}}(\omega)$ as

$$P_{\text{diff}}(\omega) = P(1 - \text{Re}\,[\gamma]). \tag{3.8}$$

Therefore, the PSDs of the common motion can be calculated as

$$P_{\text{comm}}(\omega) = P(1 + \text{Re}\,[\gamma]). \tag{3.9}$$

Finaly, CDMR defined Eq.(3.2) in case the seismic wave does not decay is represented as

$$\text{CDMR} = \sqrt{\frac{1 + \text{Re}\,[\gamma]}{1 - \text{Re}\,[\gamma]}}. \tag{3.10}$$

Eq.(3.10) indicate that CDMR can be expressed by only the coherence γ between of two points. For example, CDMR tends to be larger when γ close to 1. This means that the differential motion is more less than the common motion because the two points move together in the same direction.

3.4 Measurement of Differential Motion Reduction

3.4.1 Reduction in X-arm Scale

3.4.2 Reduction in Other Short Scale

3.5 Summary of the Chapter

Chapter 4

Geophysics Interferometer (GIF)

4.1 Overview

4.1.1 Laser Strainmeter gor Geophysics

4.1.2 Motivation in GW detectors

4.2 Working Principle

4.2.1 Asynmetric Michelson Interferometer

$$\phi = 2\pi \frac{2(l_x - l_y)}{\lambda} \sim 4\pi \frac{l_x}{\lambda} \tag{4.1}$$

$$|d\phi| = 4\pi \frac{l_x}{\lambda} \left(\left| \frac{d\lambda}{\lambda} \right| + \left| \frac{dl_x}{l_x} \right| \right) \tag{4.2}$$

4.2.2 Response to the seismic strain

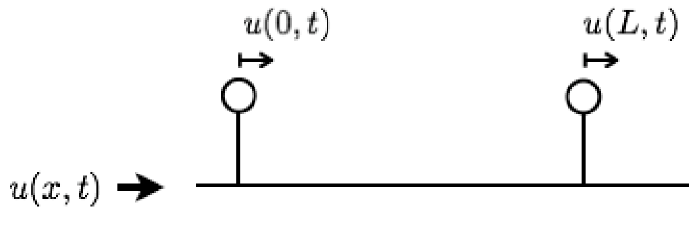

Figure 4.1: The displacements of the two points which are sparated L in X axis.

The response of the strainmeter to seismic waves have characteristics of the low pass filter. To calculate this response, it is assumed that the plane seismic waves which displacement $u(x,t)$ is represented as $u(x,t) = u_0 e^{i(\omega t - kx)}$ with angular frequency of ω and wave number of k, propagate along with the direction of the base-line of the strainmeter. The length fluctuation between two mirrors sparated with L can be expressed as

$$\begin{aligned}\Delta L(t) &\equiv u(0,t) - u(L,t) \qquad (4.3)\\ &= u(0,t) - u(0,t-\tau), \qquad (4.4)\end{aligned}$$

where $\tau = L/v$ is the time delay. The transfer function from the displacement to the length fluctuation is

$$H_{\mathrm{disp}}(s) \equiv \frac{\Delta L(s)}{u(s)} = 1 - \exp(-\tau s) \qquad (4.5)$$

Because the strain amplitude $\epsilon(x,t)$ is defined as $\epsilon(x,t) \equiv \frac{du}{dx}$, the strain

$$\begin{aligned}\epsilon(x,t) \equiv \frac{du}{dx} &= \frac{du}{dt}\frac{dt}{dx} \qquad (4.6)\\ &= u(x,t)'\frac{1}{v} \qquad (4.7)\end{aligned}$$

Therefore, the response of the strainmter to the seismic strain is given

$$H_{\mathrm{strain}}(s) \equiv \frac{\Delta L(s)}{\epsilon(s)} = \frac{\Delta L(s)}{\frac{s}{v}u(s)} = (1 - \exp(-\tau s))\,\frac{v}{s} \qquad (4.8)$$

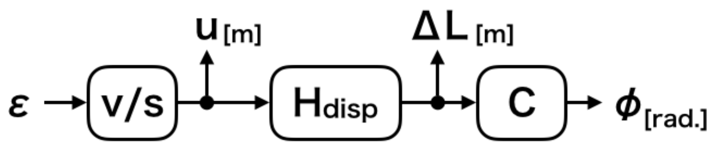

Figure 4.2

4.2.3 Signal Detection Scheme

Quadrature Phase Detection

4.2.4 Noise

どういうノイズが原理的に存在するか述べる。空気ゆらぎ、周波数雑音を述べる。

4.3 Optics

どうやって実際の干渉計を構築しているか述べる。

4.3.1 Mode Matching Optics

どういうモードマッチをして干渉計として光を干渉させているか述べる。

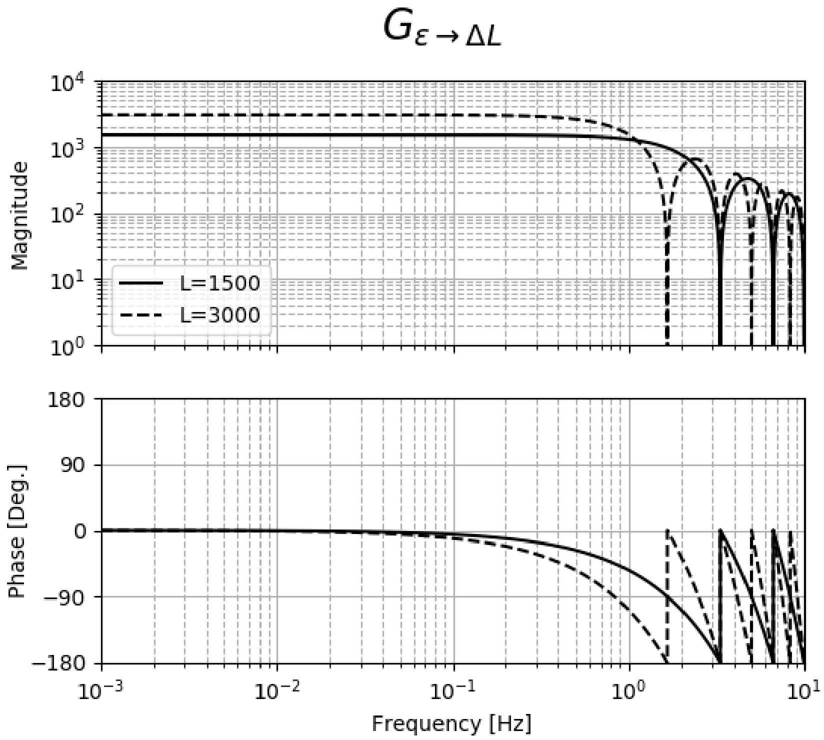

Figure 4.3

4.3.2 Frequency Stabilized Laser

どういう制御をして周波数安定をしているか述べる。

4.3.3 Core Optics

Beam Splitter

どういうミラーを使っているか述べる。

Corner Cube

どういうミラーを使っているか述べる。大きさとか表面の精度とか。

4.4 Data Aquisition System

4.4.1 ...

4.5 Summary of the Chapter

本章で述べたパラメータを表にまとめる。

Chapter 5

Arm Length Compensation System for Global Seismic Control

5.1 Basics in Vibration Isolation and Control Technique

5.1.1 Passive Vibration Isolation

Single Pendulum

Multi Pendulum

5.1.2 Active Vibration Isolation

5.1.3 Sensor Belnding Control Technique

5.1.4 2 Types Feedforward Control Techniques

Feedforward at Feedback Point

Feedforward at Error Point

5.1.5 Toward the Global Seismic Control

Overview

Suspension Point Interferometer

5.2 Difficulties in the Global Seismic Control

5.2.1 Overview

5.2.2 Actuator Range Limit

5.2.3 ...

5.2.4 ...

5.3 Arm Length Compensation Using Geophysics Interferometer

5.3.1 Concept

5.3.2 Geophysics Interferometer for Sensing the Arm Length

Chapter 6

Demonstration of Arm Length Compensation Control

6.1 Experimental Arrangement

6.1.1 ...

6.2 Results

6.2.1 ...

6.3 Discussion and Summary of the Chapter

6.3.1 Discussion

6.3.2 Summary

Chapter 7

Conculusion and Future Directions

7.1 Conclusion

7.2 Future Directions

Appendix A

Theory of Seismic Waves

A.1 Body Wave

等方弾性体中では変位 $\boldsymbol{u}$ は以下の波動方程式に従う。

$$\rho\ddot{\boldsymbol{u}} = (\lambda + 2\mu)\nabla(\nabla\cdot\boldsymbol{u}) - \mu\nabla\times(\nabla\times\boldsymbol{u}) \tag{A.1}$$

ここで ρ は媒質の密度、λ, μ はラメ定数である。

この波動方程式は縦波である P 波と横波である S 波について解くことができる。そのためにまず Helmholtz decomposition をつかって変位 $\boldsymbol{u}$ を発散成分 $\boldsymbol{u}_{\mathrm{div}}$ と回転成分 $\boldsymbol{u}_{\mathrm{rot}}$ で表す。つまり、

$$\boldsymbol{u}_{\mathrm{div}} = \nabla\phi \tag{A.2}$$
$$\boldsymbol{u}_{\mathrm{rot}} = \nabla\times\psi \tag{A.3}$$

となるスカラーポテンシャル ϕ とベクトルポテンシャル $\boldsymbol{\psi}$ が存在し、変位 $\boldsymbol{u}$ は

$$\boldsymbol{u} = \nabla\phi + \nabla\times\psi \tag{A.4}$$

と表すことができる。式 (A.1) に式 (A.4) を代入し、かつベクトル解析の公式、$\nabla\times(\nabla\times\boldsymbol{A}) = \nabla(\nabla\cdot\boldsymbol{A}) - \nabla^2\boldsymbol{A}$ を使うと、

$$\ddot{\phi} = v_L^2\nabla^2\phi \tag{A.5}$$
$$\ddot{\psi} = v_T^2\nabla^2\psi \tag{A.6}$$

のように 2 つの波動方程式を得る。ここで v_L, v_T は、

$$v_L = \sqrt{\frac{\lambda+2\mu}{\rho}},\ v_T = \sqrt{\frac{\mu}{\rho}} \tag{A.7}$$

である。

v_L, v_T らはそれぞれ縦波と横波の位相速度を表しているが、これを示す。まずスカラーポテンシャルとベクトルポテンシャルは式 (A.5)、式 (A.6) の波動方程式に従うので、これらの一般解は

$$\phi = \phi_0(\omega t - \boldsymbol{k}\cdot\boldsymbol{x}) \tag{A.8}$$
$$\boldsymbol{\psi} = \boldsymbol{\psi_0}(\omega t - \boldsymbol{k}\cdot\boldsymbol{x}) \tag{A.9}$$

で表すことができる。ここで ω, $\boldsymbol{k}$ は各周波数と波数ベクトルである。発散成分である $\boldsymbol{u}_{\mathrm{div}}$ は式 (A.2) に式 (A.8) を代入して、

$$\boldsymbol{u}_{\mathrm{div}} = \nabla\phi_0(\omega t - \boldsymbol{k}\cdot\boldsymbol{x}) = -\boldsymbol{k}\phi \tag{A.10}$$

となるので、変位の向きは波数ベクトルと平行である。つまり縦波であり P 波に相当する。一方で回転成分である $\boldsymbol{u}_{\mathrm{rot}}$ は式 (A.3) に式 (A.9) を代入して、

$$\boldsymbol{u}_{\mathrm{rot}} = \nabla\times\boldsymbol{\psi_0}(\omega t - \boldsymbol{k}\cdot\boldsymbol{x}) = -\boldsymbol{k}\times\boldsymbol{\psi} \tag{A.11}$$

となるので、変位の向きは波数ベクトルと直行している。つまり横波であり S 波に相当する。したがって v_L, v_T はそれぞれ縦波と横波の位相速度を示していることがわかった。また λ と μ は正の定数なので、

$$v_L > v_T \tag{A.12}$$

となって、縦波のほうが横波よりも速いことがわかる。

A.2 Rayleigh 波

(レイリー波の導出。)

A.3 Depth Dependence

(レイリー波の振幅が深さに依存していることを述べる。)

Bibliography

[1] T Uchiyama, K Furuta, M Ohashi, S Miyoki, O Miyakawa, and Y Saito. Excavation of an underground site for a km-scale laser interferometric gravitational-wave detector. *Classical and Quantum Gravity*, 31(22):224005, 2014. Link.

[2] Yukio Isozaki, Kazumasa Aoki, Takaaki Nakama, and Shuichi Yanai. New insight into a subduction-related orogen: a reappraisal of the geotectonic framework and evolution of the japanese islands. *Gondwana Research*, 18(1):82–105, 2010. Link.

[3] T Akutsu and et. al. Construction of kagra: an underground gravitational-wave observatory. *Progress of Theoretical and Experimental Physics*, 2018(1), 01 2018. Link.

[4] Yoichi Aso, Yuta Michimura, Kentaro Somiya, Masaki Ando, Osamu Miyakawa, Takanori Sekiguchi, Daisuke Tatsumi, and Hiroaki Yamamoto. Interferometer design of the kagra gravitational wave detector. *PHYSICAL REVIEW D Phys Rev D*, 88:043007, 2013. Link.

[5] Kentaro Somiya. Detector configuration of kagra the japanese cryogenic gravitational-wave detector. *Classical and Quantum Gravity*, 29(12):124007, jun 2012. Link.

[6] Okutomi Koki. *Development of 13.5-meter-tall Vibration Isolation System for the Main Mirrors in KAGRA*. PhD thesis, SOKENDAI, The Graduate University for Advanced Studies, 2019. Link.

[7] P Bormann. New manual of seismological observatory practice. *GFZ German Research Centre for Geosciences*, 2012. Link.

[8] RA Haubrich, WH Munk, and FE Snodgrass. Comparative spectra of microseisms and swell. *Bulletin of the Seismological Society of America*, 53(1):27–37, 1963. Link.

[9] Michael Selwyn Longuet-Higgins. A theory of the origin of microseisms. *Philosophical Transactions of the Royal Society of London. Series A, Mathematical and Physical Sciences*, 243(857):1–35, 1950. Link.

[10] Nanometrics Inc., 250 Herzberg Road Kanata, Ontario, Canada K2K 2A1. *Trillium 120Q/QA User Guide*, 04 2017.